13,12

Reversible $c(4 \times 4) \leftrightarrow (1 \times 2)$ phase transition on the Ba/Ge(100) surface controlled by oxygen adsorption and desorption

© M.V. Kuzmin, S.V. Sorokina

Ioffe Institute,
St. Petersburg, Russia

E-mail: m.kuzmin@mail.ioffe.ru

Received January 31, 2023
Revised January 31, 2023
Accepted February 1, 2023

Modified (100) surfaces of group IV semiconductors are successfully used as substrates for growing films of crystalline oxides, in particular, BaO. In this regard, it is important to understand the formation mechanisms and physicochemical properties of surface atomic structures formed on these substrates. In this work, using combined modern experimental methods, we have studied the reversible $c(4 \times 4) \leftrightarrow (1 \times 2)$ phase transition on the Ba/Ge(100) surface, which is due to the presence of oxygen atoms on it. Information about the structural and electronic properties of these surface reconstructions is obtained, and their atomic models are also proposed. The results presented are important, in particular, from the point of view of the integration of germanium into currently used silicon technologies.

Keywords: Surface, germanium, adsorbed layer, barium, oxygen, phase transition, atomic structure, scanning tunneling microscopy, photoelectron spectroscopy using synchrotron radiation.

DOI: 10.21883/PSS.2023.04.56010.14

1. Introduction

Currently germanium, along with graphene and molybdenum disulfide, is seen as one of the most promising materials to be used in existing silicon-based technology. Thus, it has a higher electron and hole mobility compared to Si and it is more attractive for the use as a current-conducting channel material in metal-oxide-semiconductor field-effect transistors [1,2]. Also, germanium is promising for the development of infrared photodiodes for silicon-based photonic integrated circuits [1,3]. The implementation of germanium in Si-based technology, however, is hindered by two significant challenges. First, the GeO_x oxide films on its surface are not stable enough and can decompose at temperatures of $\sim 300^\circ$C [4]. The second challenge is connected to the fact that Ge and Si interfaces with foreign films applied on them are rather different from each other. In particular, these differences can be illustrated by the example of epitaxial film structures of BaO/Si(100) [5] and BaO/Ge(100) [6]. These systems require a specific modification of the substrate surface prior to the growth of crystalline barium oxide film. In the case of Si(100), a 0.5 monolayer (ML) of strontium atoms has been applied on the clean surface, which leaded to the (1×2) reconstruction where broken bonds of surface atoms have been saturated by valence electrons of the adsorbate [7,8]. In turn, in the case of Ge(100) the $c(4 \times 4)$ reconstruction induced by a layer of Ba atoms has been formed on the surface followed by oxygen adsorption above it, which resulted in the formation of the O–Ba–Ge(100)(1×2) structure served as a substrate for the growth of crystalline oxide film [6]. In addition, it has been found that local defects formed in the region of BaO/Si(100) and BaO/Ge(100) interfaces are of different nature and have a significant effect on electronic and electrical properties of film structures [5,6]. Thus, from all has been said it follows that successful integration of Ge in the Si-technology requires a more detailed understanding of surface structures formed as a result of the interaction between these semiconductors and the adsorbed layers. Currently this problem is still far from being solved. Thus, for example, the atomic structure of Ba/Ge(100)$c(4 \times 4)$ and O–Ba–Ge(100)(1×2) surfaces has not been studied at all. The purpose of this study is to shed light on this issue.

In previous studies of adsorbed barium layers on the Ge(100), several reconstructions already have been reported forming in the region of submonolayer coatings, namely: in (2×3), (4×3) and $c(2 \times 6)$ structures with 1/6 ML coating, in (9×1) in the coating interval of 1/4–1/2 ML and in (6×1) with 1 ML coating [9–11]. The atomic structure of these adsorbed phases have been studied by scanning tunneling microscopy (STM) and quantum-chemical calculations based on the density functional theory. Also, it has been found that Ba atoms tend to occupy „on-top“ adsorption centers and form isolated monomers, dimers, extended chain-like structures composed of atoms of this metal, and surface phases with atoms induced in the rows of surface Ge dimers [12]. In all these structures the character of adsorption bonds is predominantly ionic [12]. However, the above-mentioned results give no ideas of the atomic and electronic structure of Ba/Ge(100)$c(4 \times 4)$ and O–Ba–Ge(100)(1×2) surfaces, which are important for the creation of oxide-germanium film structures and which this study is focused on.

2. Experiment procedure

The experiments were carried out *in situ* using two separate ultrahigh vacuum systems. The photoelectron spectra were obtained on beamline I4 at MAX-lab (Sweden) at room temperature and a residual pressure of $4 \cdot 10^{-11}$ Torr in the chamber. A SPECS Phoibos 100 analyzer was used to record the results. The energy resolution was better than 100 meV. The photon energy ($h\nu$) and emission angle of electrons relative to normal to the surface (θ_e) were varied to measure the escape depth for the sample. The solid angle of collection was $\pm 1°$ for core level spectra and $\pm 9°$ for valence band spectra. The binding energy was calibrated by means of tantalum tape cleaned in oxygen. The quantitative analysis of Ge 3*d* and Ba 4*d* spectra was performed by their decomposition to components by the least square method with a linear combination of model spin-orbit Voigt functions. The background was subtracted from the raw spectra by the Shirley method [13].

Another system (with a base pressure of $5 \cdot 10^{-11}$ Torr) was equipped with low-energy electron diffraction (LEED) optics, an Omicron STM1 scanning tunnel microscope operating at room temperature, an X-ray photoelectron spectrometer (XPS) and an ion gun for samples bombardment with ions Ar^+. The STM images were taken with tungsten tips in the direct current mode. The WSxM software package was partly used for the processing [14].

Stibium-doped *n*-type Ge(100) samples were used as substrates ($\sim 1 \cdot 10^{18} - 1 \cdot 10^{19}$ cm^{-3}). Their surfaces were cleaned by repeated cycles of ion bombardment at a temperature of 400°C followed by crystal annealing at 630°C. The cleaning was performed until sharp and bright reflections of (2×1) LEED pattern were observed. The cleanness was verified by XPS, STM and photoelectron spectroscopy using synchrotron radiation. The barium was deposited from evaporators heated by tungsten filaments. The flux was calibrated on the basis of known phase diagrams for Ba–Si(111) and Ba–Si(100) adsorption systems [15–17]. One monolayer of Ba atoms on the Ge(100) surface was referred to as the atomic concentration of $6.24 \cdot 10^{14}$ cm^{-2}, which corresponds to the density of germanium atoms on a non-reconstructed face. During the adsorbate deposition the substrate was kept at room temperature. Then it was heated at 650°C for 30 min to achieve full ordering of the surface structures. The temperature was measured by an infrared pyrometer with an accuracy of ±20°.

The adsorption of oxygen was implemented using a bleeding-in system with differential pumping-out. The bleeding into the vacuum chamber was performed using a dosing valve. Samples were held in oxygen at room temperature and a pressure of $1 \cdot 10^{-7}$ Torr. The holding time was 60 s, which corresponds to the dose of 6 L (Langmuir, $1\,\text{L} = 1 \cdot 10^{-6}$ Torr·s).

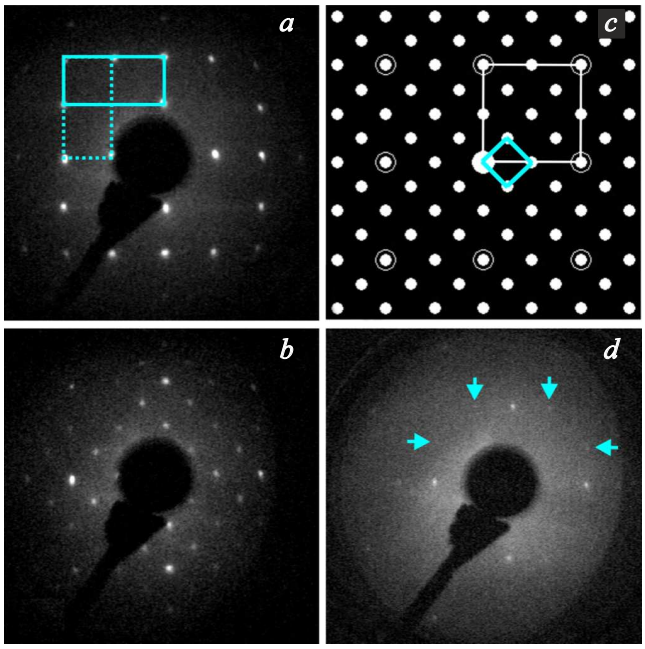

Figure 1. Diffraction patterns for different Ge(100) surfaces. *a* — clean surface. The electron energy (E_p) is 132 eV. Lines show two mutually orthogonal lattice cells of the surface superstructure. *b* — surface with adsorbed Ba layer with a coating of ~ 0.7 ML. $E_p = 116$ eV. *c* — schematic arrangement of reflections for the $c(4 \times 4)$ superstructure (filled small symbols). The (1×1) structure is shown with large unfilled symbols. Lines highlight lattice cells of both structures. *d* — surface after the adsorption of oxygen. $E_p = 136$ eV. Arrows show reflections of (1×2) structures.

3. Results

3.1. Low energy electron diffraction

Fig. 1, *a* shows a diffraction pattern taken for the Ge(100) surface free of adsorbed Ba and O atoms. This surface has a (2×1) structure at room temperature (see para. 3.2 for details). Two equivalent, mutually orthogonal lattice cells of this structure in the reciprocal space are shown in Fig. 1, *a* with solid and dashed lines.

Fig. 1, *b* shows diffraction pattern after the deposition of ~ 0.7 ML of Ba atoms onto the surface. Positions of reflections in this pattern are fully consistent with the geometry of the $c(4 \times 4)$ lattice in reciprocal space (Fig. 1, *c*). Large circles in the figure show the (1×1) structure, while small circles show the $c(4 \times 4)$ structure. Lines show lattice cells of both structures. Thus, a conclusion can be made that Ba atoms with the given coating induce the $c(4 \times 4)$ reconstruction on the germanium surface. It is worth to note that this reconstruction can be equally defined as $(2\sqrt{2} \times 2\sqrt{2})R45°$. Hereafter only the first its notation will be used throughout the text. Also, it is necessary to note that the adsorbate coating necessary to fill the $c(4 \times 4)$ reconstruction has been independently determined by not only the deposition time but also the XPS method through

comparison of intensities of Ba 4*d* lines for $c(4 \times 4)$ and (2×3) structures (the later has 1/6 ML coating [11]). On the basis of the obtained results a conclusion can be made that the amount of barium atoms in the $c(4 \times 4)$ structure is 0.70 ± 0.12 ML.

The interaction of the Ba/Ge(100)$c(4 \times 4)$ surface with oxygen results in a diffraction pattern shown in Fig. 1, *d*. It follows from this pattern that after the oxygen adsorption the reflections of the $c(4 \times 4)$ superstructure disappear completely and instead of them only weak double-periodicity reflections (shown with arrows) are observed. This means that oxygen causes the $c(4 \times 4) \rightarrow (1 \times 2)$ phase transition. It is interesting that this transition is fully reversible. If the sample produced after the interaction with oxygen is heated at 650°C for 30 min, then the diffractometer screen shows again a $c(4 \times 4)$ structure similar to that shown in Fig. 1, *b*. After this transformation, i. e. the reverse $(1 \times 2) \rightarrow c(4 \times 4)$ transition, no signal from O atoms on the surface is observed in XPS spectra. However, the intensity of Ba 4*d* lines remains unchanged. This is indicative of full recovery of the Ba/Ge(100)$c(4 \times 4)$ structure. The $c(4 \times 4) \leftrightarrow (1 \times 2)$ reversible transition caused by adsorption and desorption of oxygen can be performed an unlimited number of times. Its reversibility is indicative of the difference in strength of the adsorption bonds of O and Ba atoms with the substrate: oxygen atoms have weaker bonds than metal atoms. The removal of the former atoms from the surface at 650°C does not result in desorption of barium atoms. It is this that is responsible for the possibility of complete recovery of the $c(4 \times 4)$ reconstruction.

3.2. Scanning tunnel microscopy

Fig. 2, *a* shows a STM-image of a clean substrate taken in the mode of tunneling of electrons from filled states on the sample surface to the tip. It can be seen from the figure that the surface is formed by regularly repeated protrusions that are due to dimers of Ge atoms [18–21]. The distance between neighboring rows is $2a_{\mathrm{Ge}}$ (where $a_{\mathrm{Ge}} = 3.99$ Å being lattice constant on the Ge(100) non-reconstructed surface) and the distance between neighboring protrusions in a row is a_{Ge}. Thus, the surface shown in Fig. 2, *a* has the (2×1) structure.

A closer look at Fig. 2, *a* shows that STM-protrusions have different shapes in various areas of the surface. In the major portion of the surface, i. e. far from local defects, the protrusions have an elongated shape as can be seen in insert A'. Previously [18–21] it has been found that the axis of Ge dimers is tilted in relation to the plane of the (100) face, thus they have an asymmetric tilted shape. These dimers are subjected to rapid fluctuations between two possible states of $\mathrm{Ge}_{\uparrow}-\mathrm{Ge}_{\downarrow}$ and $\mathrm{Ge}_{\downarrow}-\mathrm{Ge}_{\uparrow}$ at room temperature (flip-flop motion). Period of these fluctuations is much less than the typical time of dimer image taking in the STM ($\sim 10^{-3}$ s). Therefore the observed protrusions represent a time-averaged pattern and are symmetric, as can be seen in insert A'.

At the same time the dynamic fluctuations of dimers can be blocked by different defects at local areas of the surface (for example, area A'' in Fig. 2, *a*), which results in stabilization of one of two tilted configurations: $\mathrm{Ge}_{\uparrow}-\mathrm{Ge}_{\downarrow}$ or $\mathrm{Ge}_{\downarrow}-\mathrm{Ge}_{\uparrow}$. Tilt of the axis of such dimers remains unchanged in time. In this case protrusions in the STM-image have asymmetric shape, as shown in insert A''. Maximum of the density of filled states of asymmetric dimers is localized near top atoms of $\mathrm{Ge}_{\uparrow}$.

Fig. 2, *b* shows a STM image of the Ge(100) surface with an adsorbed layer of Ba atoms with a coating that is slightly less than 0.7 ML. It is easy to found that formation of this layer is accompanied by a change in morphology of the surface. First, there are two adsorption phases on the surface, *H* and *L*, located at different heights. Second, domains of these phases are stretched along main crystallographic directions of [011] and $[0\bar{1}1]$ on the (100) face. This is indicative of the fact that deformations of the crystal lattice due to the difference between the covalent diameter of Ba atom (4.30 Å) and the lattice constant of the Ge(100) surface (3.99 Å) have a very high degree of spatial anisotropy. The superficial tension has a lower value in the direction of domain growth (i. e. along the elongated strips in Fig. 2, *b*) and a higher value in the perpendicular direction. Thus, the superficial tension minimization plays a significant role in the process of Ba layers growth on Ge(100).

More detailed information about the structure of the adsorbed layer can be obtained from the analysis of the atomic resolution STM-image shown in Fig. 2, *c*. It can be seen from the image that the atomic structure of the *H* and *L* adsorption phases is not the same. The *L* structure is formed by rows of weakly resolved protrusions with a distance between neighboring rows equal to $2a_{\mathrm{Ge}}$. Also, a large number of defects (vacancies) can be seen along the rows, which are manifests as dark deepenings. This structure is highly similar to the (1×2) reconstruction induced by 1/2 ML Sr on Si(100) [22]. Based on this it can be assumed that the *L* phase has an atomic structure similar to that of Sr/Si(100)(1×2).

The *H* adsorption phase has a somewhat different form. It is a regular array of protrusions that form a square lattice with a cell edge of $2\sqrt{2}a_{\mathrm{Ge}}$ and, as a consequence, it has the $c(4 \times 4)$ structure. This reconstruction covers nearly all the surface of substrate with 0.7 ML, as shown in Fig. 3, *a*. Its STM-image taken with a high resolution is shown in Fig. 3, *b*. Dashed lines in the image show the $c(4 \times 4)$ lattice cell.

To achieve a deeper understanding of the nature of (1×2) and $c(4 \times 4)$ structures, morphology of the surfaces was quantitatively analyzed in this study on the basis of STM results. The procedure of such analysis is described in detail in [23]. Fig. 4, *a* shows distribution of heights (roughness histogram) for the STM-image taken for the surface where both phases coexist (see insert in the figure). Each experimental point in this distribution characterizes the number of height repetitions in the interval from $z - \Delta z$

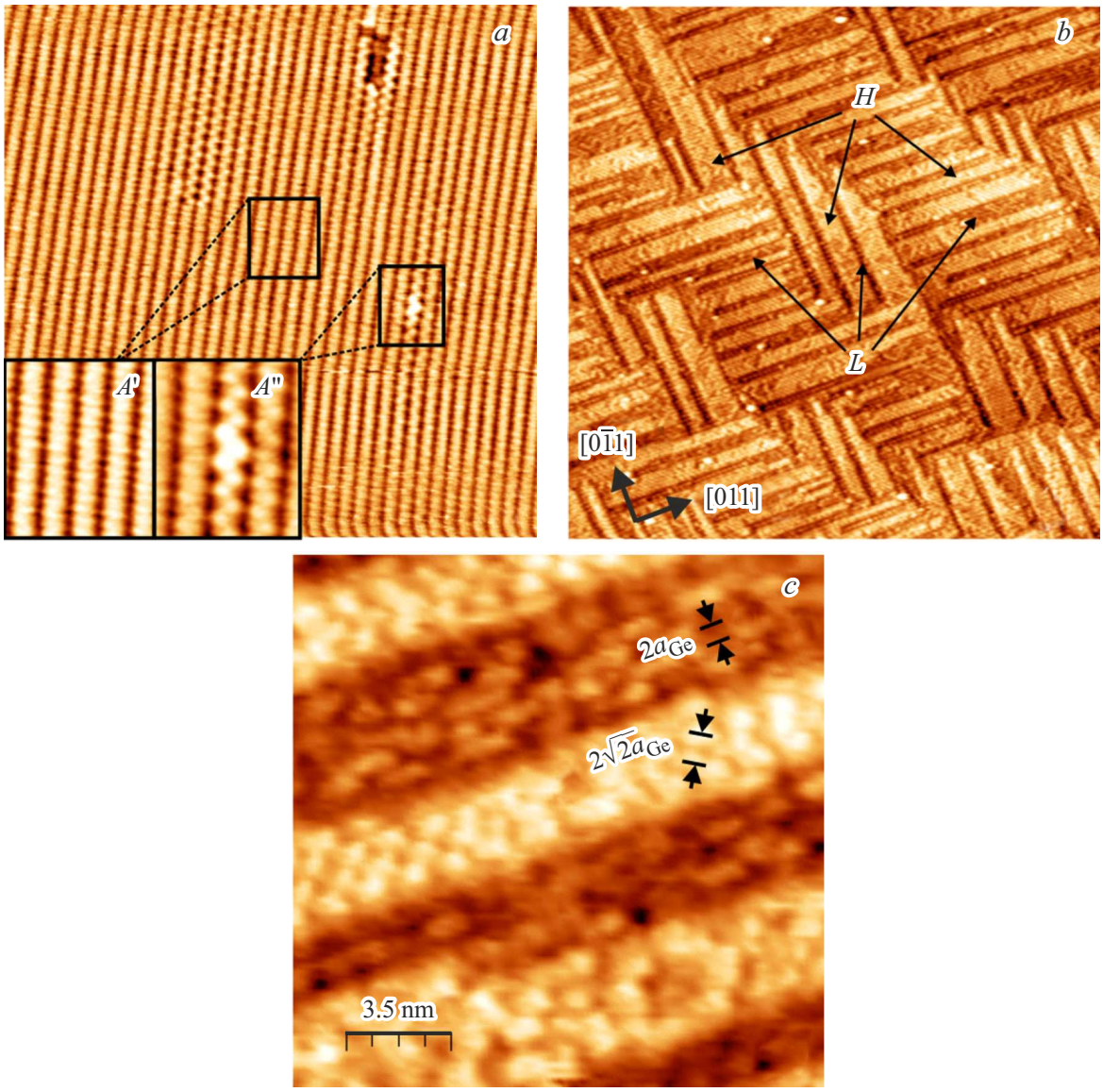

Figure 2. *a* — STM-image of clean Ge(100) surface. The bias voltage on the surface is $V_S = -1.3$ V. The tunnel current is $I_t = 0.10$ nA. Size of the images is 27×27 nm. Inserts show fragments of the image, which are zoomed in twice. *b* — STM-image of the Ba/Ge(100) surface with < 0.7 ML coating. $V_S = -1.5$ V, $I_t = 0.21$ nA. Size of the images is 150×150 nm. Arrows show *H* and *L* adsorption phases. *c* — zoomed-in area of the surface shown in image *b*. Size of the area is 18×18 nm.

to $z + \Delta z$, where $\Delta z = 5.39 \cdot 10^{-2}$ Å. As can be seen from the figure that the presented histogram is asymmetric. At the same time, the similar dependence obtained for one $c(4 \times 4)$ phase only (Fig. 4, *b*) is symmetric. Both histograms in Fig. 4 were decomposed into components using model functions of Gaussian shape (shown with solid lines). The analysis has shown that to reproduce the dependence of Fig. 4, *a*, two components are sufficient (α and β), and to reproduce the dependence of Fig. 4, *b*, one component is sufficient. The α component corresponds to the (1×2) adsorption phase, and the β component corresponds to the (4×4) phase (*L* and *H* in Fig. 2, *b*, respectively). The distance between peak maxima of α and β is 1.95 Å. This value can be interpreted as a difference in height between two phases. The above-mentioned value is considerably greater than the monoatomic step height on the Ge(100) surface (1.40 Å). Width of each peak is ≈ 2.2 Å.

Fig. 5, *a* shows STM-image of the Ba/Ge(100) surface after oxidation, i. e. after the $c(4 \times 4) \rightarrow (1 \times 2)$ phase transition. It can be seen from the figure that after the interaction with oxygen the $c(4 \times 4)$ structure is no longer observed, however, the typical morphology of the surface with elongated islands (H') and valleys between them (L'), similar to the morphology in Fig. 2, *b*, is still remained. In other words, the formation of bonds with O atoms does not change qualitatively the surface morphology. This conclusion is confirmed by the results shown in Fig. 5, *b*. This figure presents a distribution of heights for the image

shown in Fig. 5, *a*. It is composed of two components caused by H' domains (peak of β') and areas between them L' (peak α'). The distance between α' and β' is 0.98 Å. Peak α' has a width of 2.1 Å, which is close to similar values for peaks α and β in Fig. 4, *a*. Width of the peak β' is 2.9 Å. An assumption can be made that broadening of this peak is due to the adsorption of oxygen.

3.3. Photoelectron spectroscopy

3.3.1. 4*d*-Ba level. The bottom part of Fig. 6 shows normalized photoelectronic spectrum of the 4*d*-level of barium

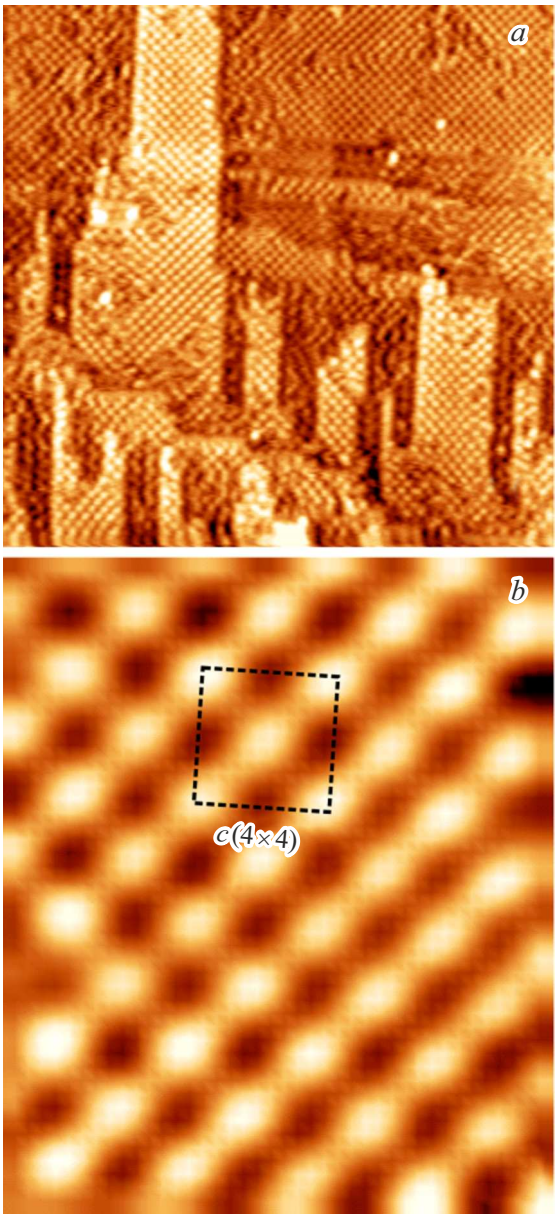

Figure 3. *a* — STM-image of the Ba/Ge(100) surface with a coating of 0.7 ML. $V_S = -2.0$ V, $I_t = 0.10$ nA. Size of the image is 64 × 64 nm. *b* — STM-image taken for the $c(4 \times 4)$ surface with high resolution. Parameters are similar to (*a*). Size of the image is 6.7 × 8.0 nm. Dashed lines show the $c(4 \times 4)$ lattice cell.

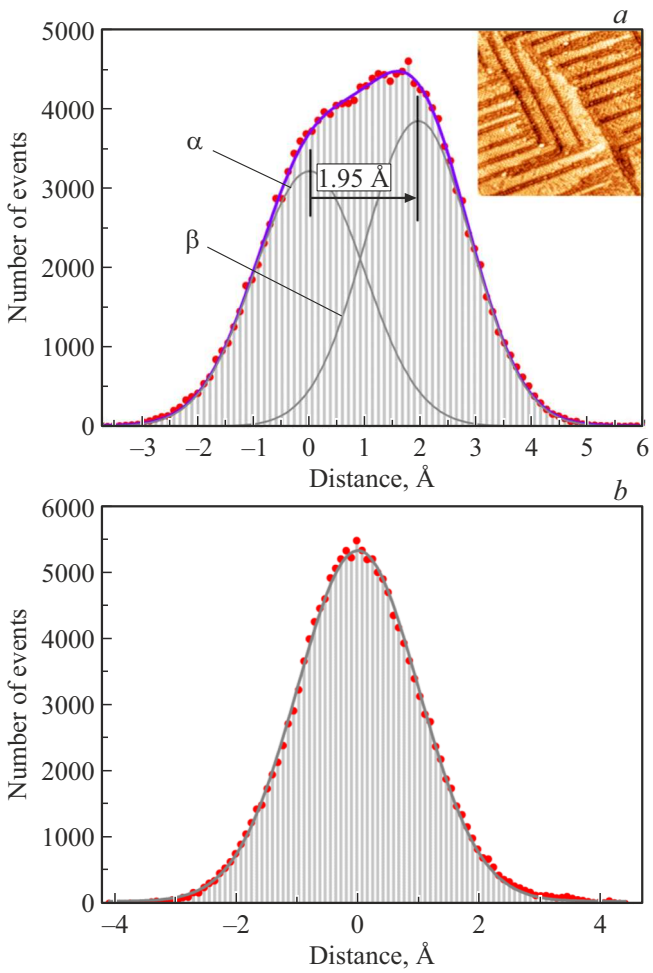

Figure 4. *a* — distribution of heights for the STM-image of the surface where barium-induced $c(4 \times 4)$ and (1×2) adsorption phases coexist. The STM-image is shown in the insert. *b* — distribution of height for the STM-image of the surface where the $c(4 \times 4)$ adsorption phase is formed (Fig. 3, *a*).

for the Ba/Ge(100)$c(4 \times 4)$ surface taken at $h\nu = 130$ eV and $\theta_e = 0°$. Light symbols show the experimental data. At the first glance, this spectrum is composed of a single spin-orbit doublet. However, a more careful analysis indicates that to reproduce well the line shape, in particular, the minimum in the energy region of 91.5–92.0 eV, two spin-orbit doublets are required: γ_1 and γ_2 (Fig. 6). This means that the $c(4 \times 4)$ structure has two non-equivalent adsorption positions for Ba atoms, which are responsible for the γ_1 and γ_2 components during the emission of electrons from the 4d-levels of these atoms. The difference in energies of these components is 0.51 eV. The ratio of their intensities is 1 : 4. If diffraction effects are not taken into account, it corresponds to the quantitative ratio of Ba atoms that occupy adsorption centers of two types. Other parameters of the decomposition of Ba 4*d*--spectra were the Loretzian and Gaussian widths of components, $\omega_L = 0.31$ and $\omega_G = 0.70$–0.72 eV, respectively, the spin-orbit splitting $(2.66 \pm 0.04$ eV) and the ratio of intensities of $4d_{3/2}$

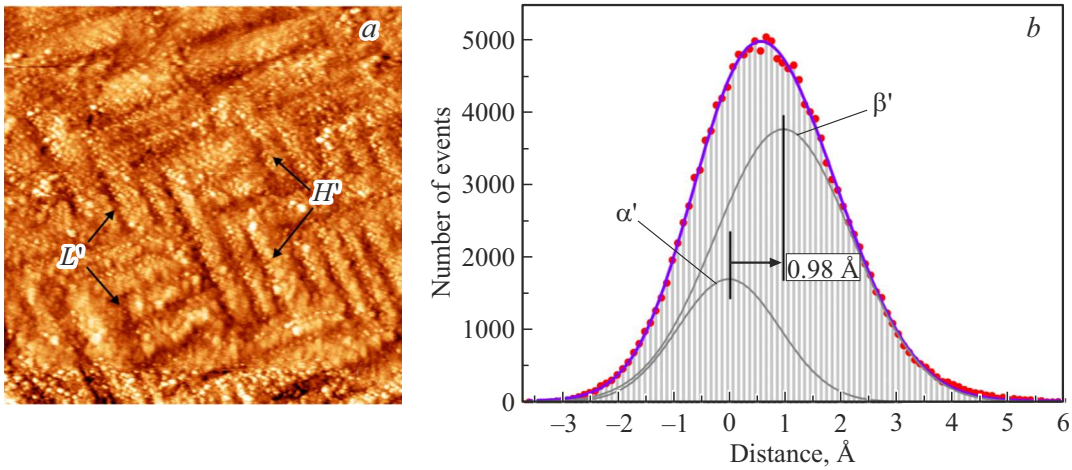

Figure 5. *a* — STM-image of the Ba/Ge(100) surface after oxidation. $V_S = -2.1$ V, $I_t = 0.21$ nA. Size of the image is 100×100 nm. *b* — distribution of heights in the STM-image (*a*).

and $4d_{5/2}$-sublevels (*the branching ratio*, 0.72 ± 0.06). The last two parameters may vary insignificantly for different surfaces and conditions of experiment [15].

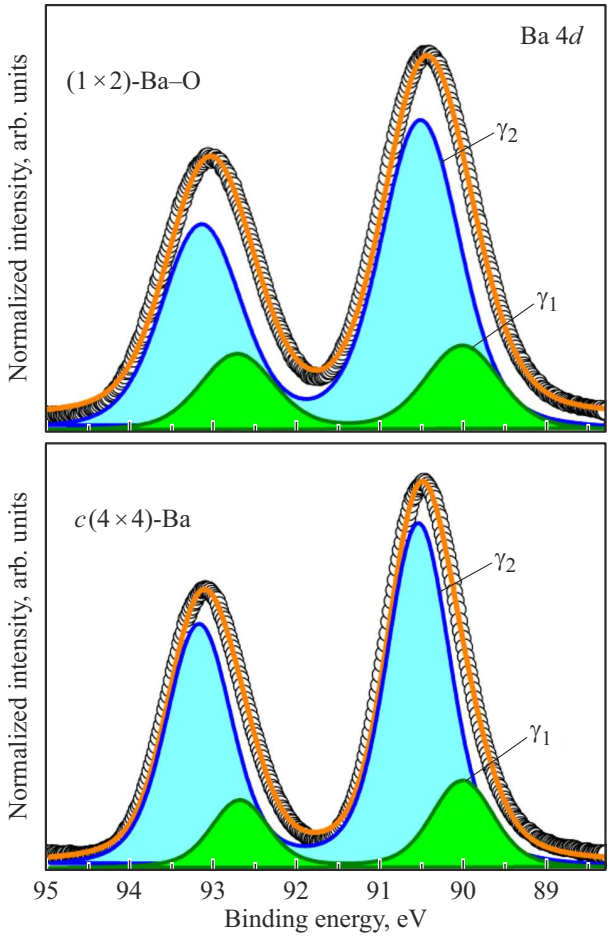

Figure 6. 4*d*--spectra of Ba before and after adsorption of oxygen on the $c(4 \times 4)$ surface. Circles show experimental data, solid lines show results of spectra decomposition to components.

The top part of Fig. 6 shows a similar spectrum after the $c(4 \times 4) \rightarrow (1 \times 2)$ phase transition induced by oxygen. Its shape is remained nearly unchanged after the oxidation. As before the interaction with oxygen, the spectrum is composed of two components, γ_1 and γ_2, with the ratio of their intensities equal to 1:4, and the difference in energy is 0.51 eV. The only difference between the spectra shown in the top and the bottom parts of Fig. 6 is that after the above-mentioned phase transition an increase in the ω_G parameter up to 0.87–0.92 eV is observed. The broadening of γ_1 and γ_2 may be caused by some increase in the degree of inhomogeneity of adsorption sites for the metal atoms. Thus, the spectroscopy of the 4*d*--level of barium is indicative of the fact that the $c(4 \times 4)-(1 \times 2)$ phase transition has almost no accompanying change in the adsorption layer of metal.

3.3.2. 3*d*-level of Ge. The left part of Fig. 7 presents normalized spectra of the 3*d*--level of Ge obtained for the $c(4 \times 4)$ reconstruction at $h\nu = 90$ eV. The bottom spectrum in this figure was taken at $\theta_e = 0°$, which corresponds to higher sensitivity to the sample volume, and the top spectrum was taken at $\theta_e = 60°$, which corresponds to higher sensitivity to the surface. The horizontal axis shows a scale of relative binding energies, which are counted in relation to the $3d_{5/2}$--sublevel of Ge in the sample body (0 eV). Round symbols show the experimental data. The quantitative analysis of these spectra has shown that they are composed of a bulk (B) and three surface components (χ_1, χ_2 and χ_3). Some sections of the spectrum could not be reproduced with the use of two surface components. And the addition of the fourth surface component to the decomposition has not resulted in any noticeable improvement in the quality of fitting. The χ_1 and χ_2 binding energies are shifted in relation to the emission from the body toward lower values by 0.62 and 0.29 eV, respectively. The χ_3 binding energy is shifted in the opposite direction (toward higher energies). Its shift is 0.10 eV. Other parameters of the decomposition are given in Table 1.

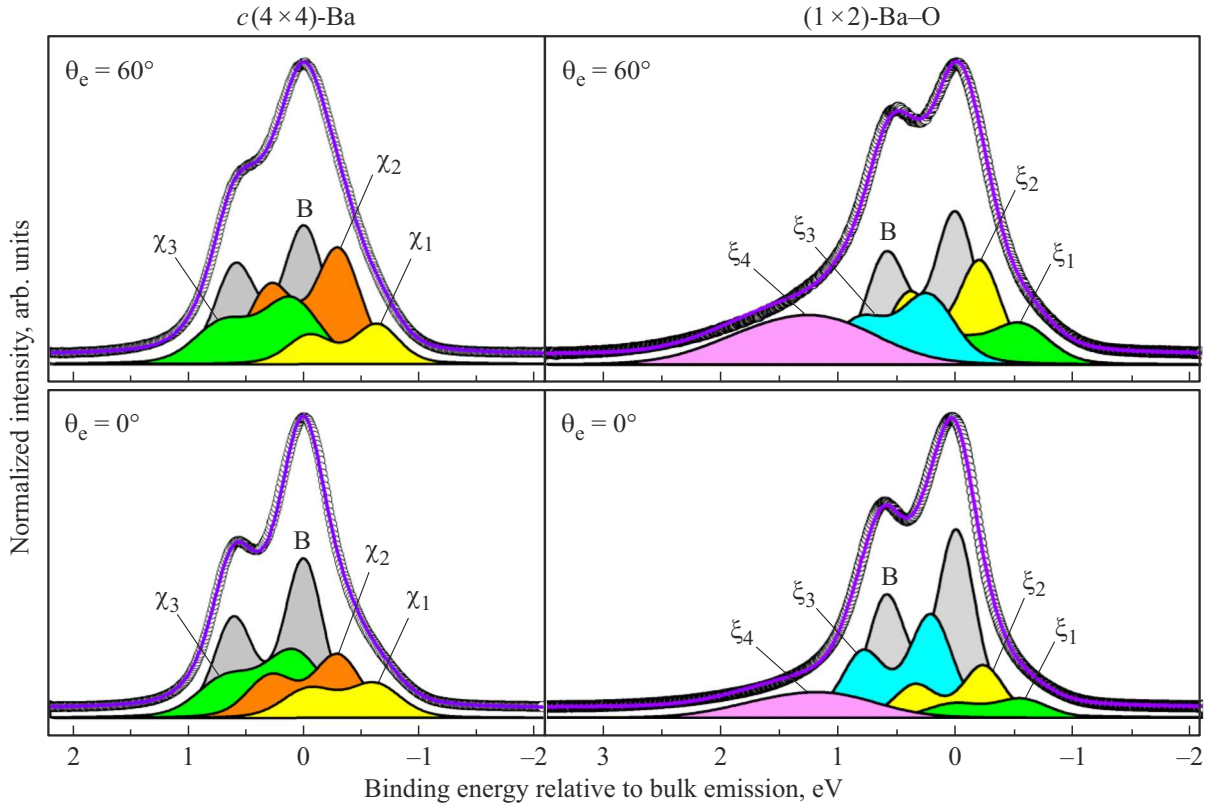

Figure 7. Normalized 3*d*--spectra of Ge before (left) and after (right) of oxygen adsorption on the $c(4 \times 4)$ surface. Open symbols show experimental results. Solid lines show results of the spectra decomposition.

Table 1. Parameters of the decomposition of 3*d*--spectra of Ge for the $c(4 \times 4)$ reconstruction. (Intensities of the χ_1, χ_2 and χ_3 components are normalized to the intensity of the *B* component and presented without brackets for the case of $\theta_e = 0^\circ$ and in brackets for the case of $\theta_e = 60^\circ$. The Lorentzian width of $\omega_L = 0.15$ eV, the spin-orbit splitting of 0.590 ± 0.02 eV and the ratio between intensities of $3d_{3/2}$-sublevel and $3d_{5/2}$--sublevel equal to 0.67 ± 0.04 were used for all components)

	B	χ_1	χ_2	χ_3
Surface shift (eV)	–	−0.62	−0.29	0.10
Relative intensity	1	0.28	0.47	0.59
		(0.31)	(0.91)	(0.63)
Gaussian width ω_L (eV)	0.32	0.41	0.39	0.50

The outcomes of the 3*d*--level spectroscopy of Ge open the possibility to make some conclusions regarding the atomic structure of the $c(4 \times 4)$ reconstruction. First, it is necessary to note that it has absolutely no tilted dimers typical for the clean Ge(100) surface. No any component shown in Fig. 7 and in Table 1 can be considered as correspondent to such dimers. Also, conspicuous is the fact that the intensity χ_2 with the transition from $\theta_e = 0^\circ$ to $\theta_e = 60^\circ$ increases by approximately two times. This is indicative of the fact that Ge atoms responsible for this component are arranged in the top layer of the substrate. The intensity χ_1 is weakly dependent on the angle θ_e, and its surface shift has a very noticeable value (−0.62 eV). The later assumes that atoms correspondent to this component are surrounded by Ba atoms to a significant extent. Hence, atoms in the top layer of Ge can be assigned to it as well. Finally, the χ_3 component has a small energy shift (0.10 eV) and is almost independent on θ_e. It is highly likely related to the atoms that are in the second layer and/or in the third layer of the substrate. The Gaussian width of this component is 20−25% greater than the χ_1 and χ_2 components (Table 1). It means that contribution to the χ_3 can be provided by Ge atoms of several types with weakly different binding energies of the 3*d*--level.

The right part of Fig. 7 shows 3*d*-spectra of Ge taken after oxygen adsorption in similar experimental conditions. It is clearly seen that the presence of oxygen on the surface causes changes in the shape of these spectra. In particular, in the region of energies of 1 eV and more an explicit „tail" appears on them. According to the performed analysis, these spectra include five components: a bulk (B) and four surface ones (ξ_1, ξ_2, ξ_3 and ξ_4). Their parameters are provided in Table 2. The ξ_1, ξ_2 and ξ_3 components have energy shifts close to the similar shifts for χ_1, χ_2 and χ_3 in Table 1. At the same time, there is no such similarity for ξ_4. This component is shifted over the energy scale toward higher binding energies by 1.05 eV. Such a shift means that it is due to Ge atoms that form bonds with O atoms. Based on the results of [24–26], a conclusion can be

made that the degree of oxidation of such Ge atoms is 1+. The Gaussian width ξ_4 is 0.96 eV. It is twice or more higher than similar values for ξ_1, ξ_2 and ξ_3 (0.34−0.48 eV). Hence, in the oxygen-stabilized (1×2) structure several different configurations of bonds between Ge^{1+} atoms and oxygen can exist.

3.3.3. Valence band. Fig. 8 shows valence spectra of the clean Ge(100) surface, the $c(4 \times 4)$ reconstruction induced on it by Ba atoms and the oxygen-stabilized (1×2) reconstruction obtained at a photon energy of $h\nu = 17$ eV. These spectra were taken at a normal angle of emission, i. e. they contain information on the electronic structure of surfaces in the neighborhood of point Γ of Brillouin zones. The most noticeable feature of the clean surface spectrum is the explicit peak marked with asterisk. This peak has an energy of 0.81 eV. It is due to the surface states that arise because of broken bonds on the bottom $Ge_{\downarrow}$ atoms of tilted dimers [27,28]. Other features of the spectrum can not be interpreted in a such unambiguous way because they can be contributed by both the surface resonances and the bulk transitions, therefore this interpretation is out of the scope of this study. It may just be noted that the analysis of spectrum shape near the Fermi level (binding energy of 0 eV) allows determining the position of valence band maximum (VBM). It is marked in the figure by arrow and

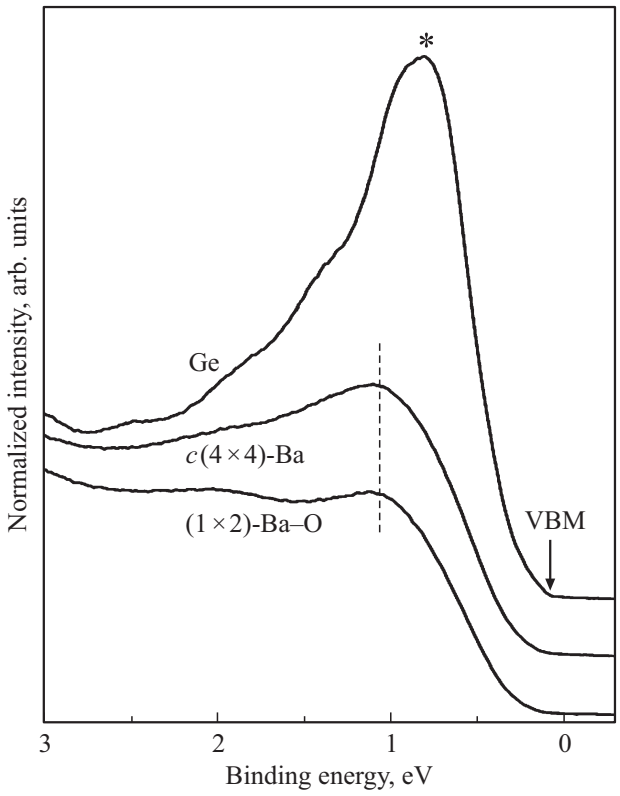

Figure 8. Valence spectra for the clean surface of the substrate, the $c(4 \times 4)$ reconstruction induced by Ba atoms and the oxygen-stabilized (1×2) reconstruction. Energies of photons are $h\nu = 17$ eV. The angle of emission is $\theta_e = 0^\circ$. The asterisk marks the feature caused by the tilted dimers on the clean surface. The arrow shows the valence band maximum (VBM).

Table 2. Parameters of the decomposition of 3*d*--spectra for Ge obtained after oxygen adsorption on the $c(4 \times 4)$ surface. (Intensities of the ξ_1, ξ_2, ξ_3 and ξ_4 components are normalized to the intensity of the B component and presented without brackets for the case of $\theta_e = 0^\circ$ and in brackets for the case of $\theta_e = 60^\circ$. The Lorentzian width, the spin-orbit splitting and the ration between intensities of $3d_{3/2}$ and $3d_{5/2}$-sublevels are similar to those specified in Table 1)

	B	ξ_1	ξ_2	ξ_3	ξ_4
Surface shear (eV)	–	−0.55	−0.22	0.23	1.05
Relative Intensity	1	0.14 (0.36)	0.30 (0.71)	0.60 (0.58)	0.25 (0.62)
Gaussian width ω_L (eV)	0.32	0.48	0.34	0.41	0.96

is 0.07−0.10 eV below the Fermi level. This value is well consistent with the results of [29,30]. VBM of the Ge(100) surface is due to the states that are related to the crystal volume.

The most important change in spectra with the formation of $c(4 \times 4)$ and (1×2) reconstructions is the disappearance of the feature marked with asterisk. It means that there are no more tilted dimers of Ge on the germanium surface. This conclusion is fully consistent with the results of photoelectron spectroscopy of the 3*d*--level of Ge (subsection 3.3.2). At the same time, the VBM has almost no shift, which is a confirmation of the bulk origin of its causing states.

4. Discussion

Below are considered atomic structures for the $c(4 \times 4)$ surface induced by Ba atoms and the (1×2) surface induced by Ba and O atoms. According to experimental results (section 3), the model of $c(4 \times 4)$ should meet the following conditions:

a) barium coating is 0.70 ± 0.12 ML;

b) Ba atoms occupy adsorption positions of two types;

c) ratio of Ba atoms in these positions is 1 : 4;

d) top atomic layer of Ge includes two non-equivalent types of atoms, which ratio is 1 : 3;

e) the $c(4 \times 4)$ reconstruction is localized 1.95 Å above the (1×2) reconstruction, which is barium-induced as well.

It is reasonable to start creation of the $c(4 \times 4)$ model from the arrangement of 1/2 ML atoms of Ba on the Ge(100) surface and consideration of the Ba/Ge(100)(1×2) structure. As STM-images of the Ba/Ge(100)(1×2) and Sr/Si(100)(1×2) surfaces are very similar to each other (see section 3.2), the model suggested for Sr/Si(100)(1×2) [22] can be used for the case of barium as well (Fig. 9, *a*). It is formed by rows of symmetric dimers of Ge. Chains of Ba atoms occupying adsorption positions of valley bridge type are located in the grooves between these rows. In this atomic configuration an exchange covalence interaction arises between electropositive

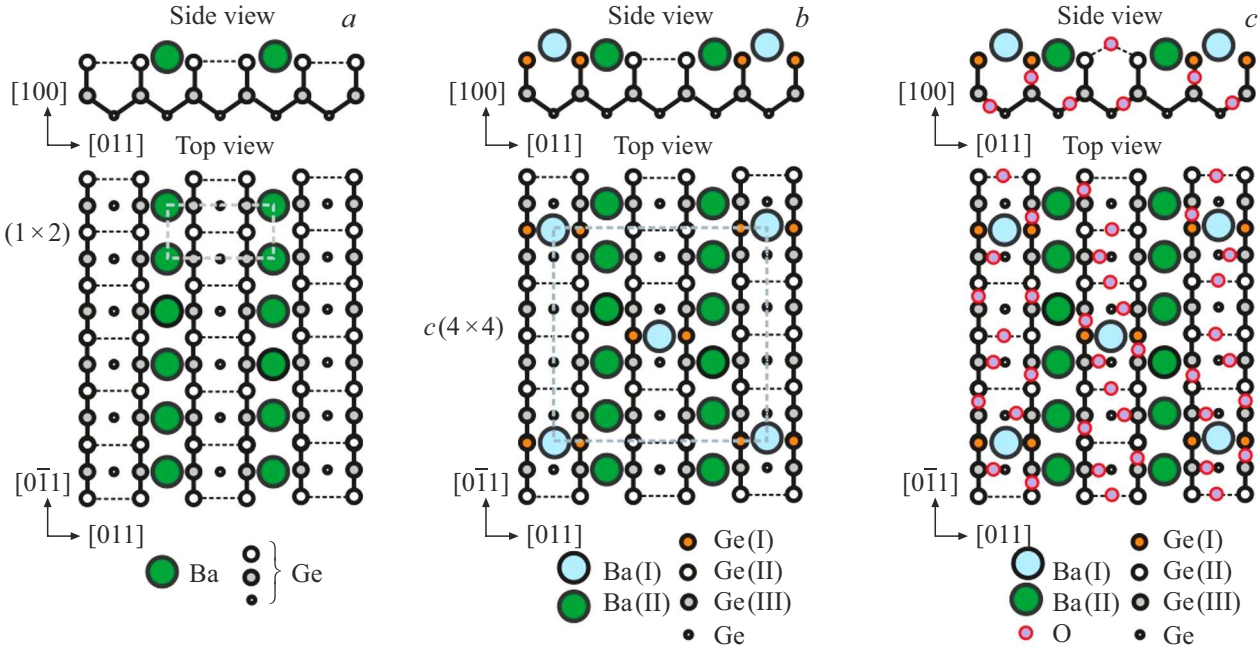

Figure 9. Atomic models for the Ba/Ge(100) and O−Ba−Ge(100) surfaces. *a* — the Ba/Ge(100)(1×2) reconstruction. Coating of the adsorbate is 0.5 ML. *b* — Ba/Ge(100)$c(4 \times 4)$ reconstruction. Coating of the adsorbate is 0.625 ML. *c* — O-Ba-Ge(100)$c(1 \times 2)$ reconstruction. The barium coating is 0.625 ML. Dashed lines outline lattice cells.

atoms of the adsorbate and electronegative atoms of the top layer of the substrate, which results in the situation that broken bonds of semiconductor atoms (one such bond per each atom) are completely saturated by s electrons from the atoms of metal (two electrons per each atom). Using the rule for electron counting, it is easy to determine that even numbers of valence electrons of the substrate and adsorbate atoms are attributable to each (1×2) lattice cell (highlighted in Fig. 9, *a* by grey dashed lines) and, as a consequence, the surface shown in this figure should be of non-metal character. It is important to note that two electrons from the adsorbed layer are attributable per one surface dimer in this structure. According to the rule of symmetrization of dimers [31], in this case tilted dimers should be transformed to symmetric ones.

The (1×2) model in Fig. 9, *a* is the starting point for building up the $c(4 \times 4)$ atomic structure. It is logical to assume that this structure (Fig. 9, *b*) is formed by adding 0.125 ML of barium atoms (denoted as Ba(I)) to the (1×2) model with a coating of 0.5 ML of Ba(II) atoms. Ba(I) atoms occupy adsorption centers of the „bridge“ type in rows of dimers (*dimer bridge*), and their arrangement defines geometry of the $c(4 \times 4)$ lattice cell. Thus, in the structure suggested in Fig. 9, *b*, Ba(I) and Ba(II) atoms are localized at different heights and their quantitative ratio is 1 : 4, which is consistent with the experimental results.

The structure shown in Fig. 9, *b* also helps to explain the presence of two types of Ge in the first layer. Ge(I) atoms can be bound to both Ba(I) atoms and Ba(II) atoms. In contrast to them, Ge(II) atoms can be bound to Ba(II) atoms only. It can be expected that the charge transfer from the adsorbate layer to Ge(I) atoms is stronger than that to Ge(II) atoms. Therefore, it is logical to assume that the χ_1 component in Fig. 7 is due to Ge(I) atoms and the χ_2 component is due to Ge(II) atoms. The ratio of these atoms in the structure shown in Fig. 9, *b* is 1 : 3, which is confirmed by the experiment (section 3.3.2).

Finally, the question arises, how oxygen interacts with the $c(4 \times 4)$ surface at the $c(4 \times 4) \rightarrow (1 \times 2)$ phase transition. As Ba 4*d* spectra are almost not transformed after the oxidation, it can be expected that Ba−O bonds are not formed at all and that oxygen is bound to Ge atoms only. The later is confirmed by the presence of the χ_4 component in 3*d* spectra of Ge in Fig. 7. Taking into account the degree of oxidation (1+) of Ge atoms on the (1×2) surface (see section 3.3.2), as well as length and bond angle of Ge−O−Ge (1.78 Å and 131° , respectively [32]), an assumption can be made regarding possible sites of oxygen atoms implanted into the $c(4 \times 4)$ reconstruction. They are shown in Fig. 9, *c*. The formation of Ge−O bonds along the rows of germanium dimers may result in the loss of the $\times 4$ periodicity on the oxidized surface. At the same time, the $\times 2$ periodicity may be kept. It is due to the arrangement of rows of Ba(II) atoms. When the sample is heated to 650°C, break of the formed Ge−O bonds takes place, oxygen is desorbed to vacuum and the $c(4 \times 4)$ structure is recovered.

5. Conclusion

The reversible $c(4 \times 4) \leftrightarrow (1 \times 2)$ phase transition on the Ba/Ge(100) surface governed by the adsorption and

desorption of oxygen has been studied by methods of LEED, STM and photoelectron spectroscopy. It is found that the $c(4 \times 4)$ reconstruction induced by barium atoms has an adsorption coating of 0.70 ± 0.12 ML. When interacting with oxygen, it is transformed to the (1×2) structure stabilized by O atoms. Then, with heating up to 650°C oxygen is desorbed from the surface, which can be resulted in complete recovery of the $c(4 \times 4)$ reconstruction. Structural properties of both adsorption phases are investigated in detail and models are suggested that allow for a consistent explanation of their atomic structure. In particular, it is shown that Ba atoms in the $c(4 \times 4)$ structure occupy adsorption centers of two types. After the adsorption of oxygen, the type of adsorption sites for these atoms remains almost unchanged. At the same time, Ge atoms form bonds with oxygen, which degree of oxidation is 1+. The strength of these bonds is relatively high, because they can be disrupted only at 650°C. It is considerably higher than the strength of Ge−O bonds formed as a result of oxidation of pure Ge(100) surface.

Conflict of interest

The authors declare that they have no conflict of interest.

References

[1] R.M. Wallace, P.C. McIntyre, J. Kim, Y. Nishi. MRS Bull. **34**, *7*, 493 (2009).
[2] Y. Kamata. Mater. Today **11**, *1*, 30 (2008).
[3] P. Vines, K. Kuzmenko, J. Kirdoda, D.C.S. Dumas, M.M. Mirza, R.W. Millar, D.J. Paul, G.S. Buller. Nature Commun. **10**, 1086-9 (2019).
[4] K. Kato, N. Taoka, M. Sakashita, O. Nakatsuka, S. Zaima. Appl. Phys. Lett. **107**, 102102 (2015).
[5] M. Kuzmin, P. Laukkanen, M.P.J. Punkkinen, M. Yasir, M. Tuominen, J. Dahl, J.J.K. Lång, J. Mäkelä, K. Kokko. Phys. Rev. B **90**, 235405 (2014).
[6] M. Kuzmin, P. Laukkanen, M. Yasir, J. Mäkelä, M. Tuominen, J. Dahl, M.P.J. Punkkinen, K. Kokko, H.-P. Hedman, J. Moon, R. Punkkinen, V. Polojärvi, V.-M. Korpijärvi, M. Guina. Phys. Rev. B **92**, 165311 (2015).
[7] C.J. Först, C.R. Ashman, K. Schwarz, P.E. Blöchl. Nature **427**, 53 (2004).
[8] J.W. Reiner, K.F. Garrity, F.J. Walker, S. Ismail-Beigi, C.H. Ahn. Phys. Rev. Lett. **101**, 105503 (2008).
[9] B.R. Lukanov, J.W. Reiner, F.J. Walker, C.H. Ahn, E.I. Altman. Phys. Rev. B **84**, 075330 (2011).
[10] W. Koczorowski, A. Puchalska, T. Grzela, L. Jurczyszyn, S.R. Schofield, R. Czajka, N.J. Curson, M.W. Radny. Phys. Rev. B **93**, 195304 (2016).
[11] W. Koczorowskia, T. Grzela, A. Puchalska, M.W. Radny, L. Jurczyszyn, S.R. Schofield, R. Czajka, N.J. Curson. Appl. Surf. Sci. **435**, 438 (2018).
[12] A. Puchalska, L. Jurczyszyn, W. Koczorowski, R. Czajka, M.W. Radny. Appl. Surf. Sci. **481**, 1474 (2019).
[13] A. Proctor, P.M.A. Sherwood. Anal. Chem. **54**, 13 (1982).
[14] I. Horca, R. Fernández, J.M. Gómez-Rodríguez, J. Cochero, J. Gómez-Herrero, A.M. Baro. Rev. Sci. Instrum. **78**, 013705 (2007).
[15] T. Okuda, K.-S. An, A. Harasawa, T. Kinoshita. Phys. Rev. B **71**, 085317 (2005).
[16] W.C. Fan, A. Ignatiev. Surf. Sci. **253**, 297 (1991).
[17] D. Vlachos, M. Kamaratos, C. Papageorgopoulos. Solid State Commun. **90**, *3*, 175 (1994).
[18] J.A. Kubby, J.E. Griffith, R.S. Becker, J.S. Vickers. Phys. Rev. B **36**, 6079 (1987).
[19] O. Gurlu, H.J.W. Zandvliet, B. Poelsema. Phys. Rev. Lett. **93**, 066101 (2004).
[20] M.W. Radny, G.A. Shah, S.R. Schofield, P.V. Smith, N.J. Curson. Phys. Rev. Lett. **100**, 246807 (2008).
[21] B. Yan, C. Yam, A. Luisa da Rosa, T. Frauenheim. Phys. Rev. Lett. **103**, 189701 (2009).
[22] M. Kuzmin, P. Laukkanen, M.P.J. Punkkinen, J. Mäelä, M. Yasir, J. Dahl, M. Tuominen, K. Kokko. Surf. Sci. **646**, 140 (2016).
[23] M.V. Kuzmin, M.A. Mitsev, ZhTF **90**, *8*, 1359 (2020) (in Russian).
[24] D. Schmeisser, R.D. Schnell, A. Bogen, F.J. Himpsel, G. Landgren, J.F. Morar. Surf. Sci. **172**, *2*, 455 (1986).
[25] K. Prabhakaran, T. Ogino. Surf. Sci. **325**, *1*, 263 (1995).
[26] K.-I. Seo, P.C. McIntyre, S. Sun, D.-I. Lee, P. Pianetta, K.C. Saraswat. Appl. Phys. Lett. **87**, 042902 (2005).
[27] E. Landemark, R.I.G. Uhrberg. Surf. Sci. Lett. **236**, L359 (1990).
[28] E. Landernark, C.J. Karlsson, L.S.O. Johansson, R.I.G. Uhrberg. Phys. Rev. B **49**, 16523 (1994).
[29] H. Seo, R.C. Hatch, P. Ponath, M. Choi, A.B. Posadas, A.A. Demkov. Phys. Rev. B **89**, 115318 (2014).
[30] M. Kuzmin, P. Laukkanen, J. MÁkelä, M. Tuominen, M. Yasir, J. Dahl, M.P.J. Punkkinen, K. Kokko. Phys. Rev. B **94**, 035421 (2016).
[31] M. Kuzmin, M.P.J. Punkkinen, P. Laukkanen, R.E. Perälä, V. Tuominen, J.J.K. Lång, M. Ahola-Tuomi, J. Dahl, T. Balasubramanian, B. Johansson, L. Vitos, I.J. Väyrynen. Phys. Rev. B **82**, 113302 (2010).
[32] P. Broqvist, J. Felix Binder, A. Pasquarello. Microelectron. Eng. **86**, 1589 (2009).

Translated by Y.Alekseev